Er:LiYF4 planar waveguide laser at 2.8 μm

Ji Eun Bae, Pavel Loiko, Simone Normani, Gurvan Brasse, Abdelmjid Benayad, Alain Braud, Patrice Camy

Er:$LiYF_4$ planar waveguide laser at 2.8 µm

Ji Eun Bae, Pavel Loiko, Simone Normani, Gurvan Brasse, Abdelmjid Benayad, Alain Braud, and Patrice Camy[a)]

Centre de Recherche sur les Ions, les Matériaux et la Photonique (CIMAP), UMR 6252 CEA-CNRS-ENSICAEN, Université de Caen Normandie, 6 Boulevard Maréchal Juin, 14050 Caen Cedex 4, France

[a)]Author to whom correspondence should be addressed: patrice.camy@ensicaen.fr

We report on a mid-infrared Erbium planar waveguide laser operating on the $^4I_{11/2} \rightarrow {}^4I_{13/2}$ transition. It employs a heavily-doped 10.6 at.% Er^{3+}:$LiYF_4$ single-crystalline layer grown by Liquid-Phase Epitaxy (LPE). The waveguide laser delivers a maximum output power of 191 mW at ~2809 nm with a slope efficiency of 15%, a linear polarization and a laser threshold of 134 mW. The waveguide propagation losses are 0.4±0.2 dB/cm. The polarized spectroscopic properties of Er^{3+}:$LiYF_4$ layers are also investigated. The stimulated-emission cross-section of Er^{3+} ions amounts to 0.87×10^{-20} cm^2 at 2809 nm for π-polarization. Er^{3+}:$LiYF_4$ epitaxial layers represent a promising platform for integrated low-loss mid-infrared light sources.

Waveguide (WG) geometry of laser gain media has emerged as one of the most promising candidates for miniaturization of solid-state laser sources. It provides a great potential for diverse applications, including on-chip integrated light sources and high-repetition-rate mode-locked lasers.[1-3] Such ultrafast WG lasers remain unexplored in the mid-infrared spectral range (at 3 µm and beyond) despite their specific niches including environmental gas detection, biosensing, and pumping of laser sources emitting at even longer wavelengths, e.g., supercontinuum sources.[4,5]

So far, the majority of studies on mid-infrared WG lasers relied on the Ultrafast Laser Inscription (ULI) method enabling fabrication of channel WGs in the depressed cladding (type III) geometry[6] based on various transparent materials, namely crystals, ceramics, and glasses, see Table I. One group of such lasers consists of transition-metal-ion doped (Cr^{2+}, Fe^{2+}) zinc chalcogenides (ZnS and ZnSe) featuring extremely broad emission bands. Berry *et al.* developed a 6-mm-long Cr^{2+}:ZnSe WG laser delivering 1.7 W at 2.50 µm with a slope efficiency of 23% when pumping by a commercial Tm-fiber laser.[7] Macdonald *et al.* reported on a broadband wavelength tuning (2.08-2.78 µm) of a similar laser in the extended cavity configuration.[8] By using Fe^{2+}:ZnSe WGs cooled to 77 K and an Er:YAG laser as pump source, Lancaster *et al.* achieved 76 mW at a longer wavelength of 4.12 µm with a slope efficiency of 15%.[9] However, the synthesis of these gain media with high optical quality is challenging and they suffer from relatively low laser-induced damage thresholds and the need for special pump sources.

The second group consists of rare-earth ion based (Er^{3+}, Ho^{3+}) lasers. Holmium ions (Ho^{3+}) provide emission near 2.9 µm due to the $^5I_6 \rightarrow {}^5I_7$ transition. Lancaster *et al.* developed a 18-mm-long Ho,Pr:ZBLAN glass WG laser diode-pumped at 1.16 µm generating 170 mW at 2.87 µm with a slope efficiency of 21%.[10] Despite the appealing spectroscopic properties of Ho:ZBLAN glasses related to their low phonon energy behavior and broadband transparency, their low thermal conductivity does not allow for power scaling.

TABLE I. Output characteristics[a] of mid-infrared waveguide lasers reported so far.

Material	[b]	P_{out}, mW	η, %	P_{th}, mW	λ_L, µm	λ_P, µm	Ref.
Cr:ZnS	ULI	78	8.6	29	2.24	1.92	[11]
Cr:ZnSe	ULI	1700	23	>200	2.50	1.91	[7]
Cr:ZnSe	ULI	285	45	200	2.49	1.93	[12]
Fe:ZnSe	ULI	76	11	210	4.12	2.94	[9]
Ho:ZBLAN	ULI	27	19.5	28	2.91	1.15	[13]
Ho,Pr:ZBLAN	ULI	170	21	104	2.87	1.16	[10]
Er:Y_2O_3	ULI	123.5	21	155	2.72	0.98	[14]
Er:$LiYF_4$	ULI	66	19.6	120	2.81	0.80	[15]
Er:$LiYF_4$	LPE	191	15	134	2.81	0.97	[c]

[a]P_{out} – maximum output power, η – slope efficiency, P_{th} – laser threshold, λ_L and λ_P – laser and pump wavelengths, respectively. [b]ULI – ultrafast laser inscription, LPE – Liquid Phase Epitaxy. [c]This work.

Erbium ions (Er^{3+}) are known for their mid-infrared emission at ~2.8 µm (the $^4I_{11/2} \rightarrow {}^4I_{13/2}$ transition) which is of interest for bio-medical applications. They can be efficiently pumped at 0.96 µm by commercial InGaAs laser diodes or Yb-fiber lasers. However, the demonstration of ultrashort pulse generation from 3-µm Er lasers is challenging because of the structured water vapor absorption in this spectral range.[4,16] This issue can be overcome by implementing the compact monolithic WG laser design. As host materials for Er^{3+} doping targeting 2.8-µm laser development, fluoride crystals such as lithium yttrium fluoride ($LiYF_4$) are in the spotlight as they combine (i) low phonon energies leading to long upper laser level ($^4I_{11/2}$) lifetimes and, thus, low laser thresholds, (ii) high Er^{3+} doping levels boosting the energy-transfer upconversion (ETU, $^4I_{13/2} + {}^4I_{13/2} \rightarrow {}^4I_{15/2} + {}^4I_{9/2}$) overcoming the bottleneck effect, and (iii) high thermal conductivity allowing for power scaling.[17]

2.8-µm Erbium WG lasers fabricated by ULI were recently demonstrated.[14,15] Tian *et al.* reported on a 7-mm-long Er:Y_2O_3 ceramic WG laser delivering 124 mW at 2.72 µm with a slope efficiency of 21% pumping by a 976-nm diode.[14]

Planar WGs are capable of inherent definite refractive index differences between the active layer and the surrounding materials such as the undoped substrate and air

(or cladding). They provide sufficient confinement conditions without rigorous control of the refractive index modification as in the case of the ULI method. The planar WG geometry displays the advantage of direct integration with saturable absorbers for pulsed operation and further design of channel guides via reactive ion etching or diamond-saw dicing.[18-20] Williams *et al.* have demonstrated a proof of concept for a mid-infrared planar WG laser with a Cr^{2+}:ZnSe thin film grown by pulsed laser deposition on a sapphire substrate.[21] The laser action in the gain switching regime at 2.6 μm was achieved.

Liquid-Phase Epitaxy (LPE) is a relevant method for producing low-loss (down to 0.1 dB/cm), single-crystalline well oriented rare-earth-doped waveguiding layers with easily managed refractive index contrast.[19,22,23] LPE is well developed for $LiYF_4$, and planar WG lasers covering a broad spectral range from visible to near-infrared (up to 2.1 μm) have been reported based on this fluoride material platform. In the present work, we report on the first 2.8-μm Er:$LiYF_4$ planar WG laser using heavily Er^{3+}-doped $LiYF_4$ epitaxial layers. Their polarized spectroscopic properties are also studied.

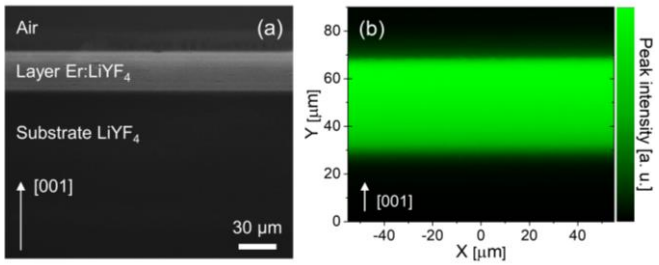

FIG. 1. Er:$LiYF_4$ epitaxial layer: (a) a confocal microscope image of a polished end-facet of the epitaxy; (b) micro-luminescence mapping of the emission peak intensity at 551 nm (the $^4S_{3/2} \rightarrow {}^4I_{15/2}$ transition), λ_{exc}=488 nm, π-polarization.

Single-crystalline Er^{3+}-doped $LiYF_4$ layers were grown on undoped [001] oriented bulk $LiYF_4$ substrates by LPE. Lithium fluoride (LiF) was used as a solvent or as a self-flux compound and the growth batch composition was 73 LiF – 27 YF_3 (mol%).[23] The Er^{3+} doping level was 11 at.% (with respect to Y^{3+}). The growth temperature was 745.5 °C (an apparent supercooling of 0.5 °C) and the growth duration was 45 min. The growth rate was about ~1 μm/min. The epitaxial layers were polished down to the desired thickness of 40 μm with low surface roughness in the nm range. The confocal laser microscope image of a polished end-facet of the epitaxy is shown in Fig. 1(a) revealing a free of cracks and inclusions layer and a clean substrate/layer interface. The μ-luminescence mapping across the sample end-facet was performed for polarized light, Fig. 1(b). The intensity of the emission peak at ~551 nm (the $^4S_{3/2} \rightarrow {}^4I_{15/2}$ transition) was mapped with a spatial resolution of 0.5 μm. It confirmed a uniform distribution of Er^{3+} ions in the layer.

Prior to WG laser experiments, polarized spectroscopic properties of Er^{3+} ions in the $LiYF_4$ epitaxial layer were addressed. The polarized absorption spectra were measured by coupling the attenuated broadband output (~40 mW) of a high-brightness supercontinuum source (ELECTRO VIS 470, LEUKOS Laser) into the layer and detecting the transmitted light by an optical spectrum analyzer (OSA, Ando AQ-6315E), see Fig. 2(b). A reference measurement through the undoped substrate was used to calibrate the setup. For the $^4I_{15/2} \rightarrow {}^4I_{11/2}$ pump transition, the peak absorption coefficient is 9.2 cm^{-1} at 971.7 nm and the absorption bandwidth (FWHM) is 4.1 nm for π polarization. Based on the absorption cross-sections for bulk crystals, the actual Er^{3+} doping level was estimated to be 10.6±1 at.% (Er^{3+} ion density: $N_{Er} = 14.6\times10^{20}$ at/cm^3, segregation coefficient: K_{Er} = 0.96). The polarized mid-infrared luminescence spectra were measured using an OSA (AQ6376, Yokogawa) purged by N_2 gas. The stimulated-emission (SE) cross-sections, σ_{SE}, for the $^4I_{11/2} \rightarrow {}^4I_{13/2}$ transition were calculated via the Füchtbauer-Ladenburg formula using the radiative lifetime of the $^4I_{11/2}$ state (τ_{rad} = 6.7 ms) and the luminescence branching ratio ($\beta_{JJ'}$ = 0.15) obtained by the Judd-Ofelt theory.[24] The Er:$LiYF_4$ layer exhibits intense and strongly polarized emission spanning from 2.65 to 2.9 μm, Fig. 2(c). Higher emission intensity is observed for π-polarization and the peak σ_{SE} values at the observed laser wavelengths are 1.91×10^{-20} cm^2 at 2663 nm, 1.29×10^{-20} cm^2 at 2718 nm, and 0.87×10^{-20} cm^2 at 2809 nm. The polarized emission properties of the Er:$LiYF_4$ layer confirm its proper orientation. The luminescence decay was studied under resonant excitation using a ns optical parametric oscillator (Horizon, Continuum), 1/4 m monochromator, an InGaAs photodetector and an 8-GHz digital oscilloscope (DSA70804B, Tektronix). The average luminescence lifetimes $\langle\tau_{lum}\rangle$ of the $^4I_{11/2}$ and $^4I_{13/2}$ Er^{3+} manifolds are 3.40 ms and 6.31 ms, respectively, Fig. 2(d).

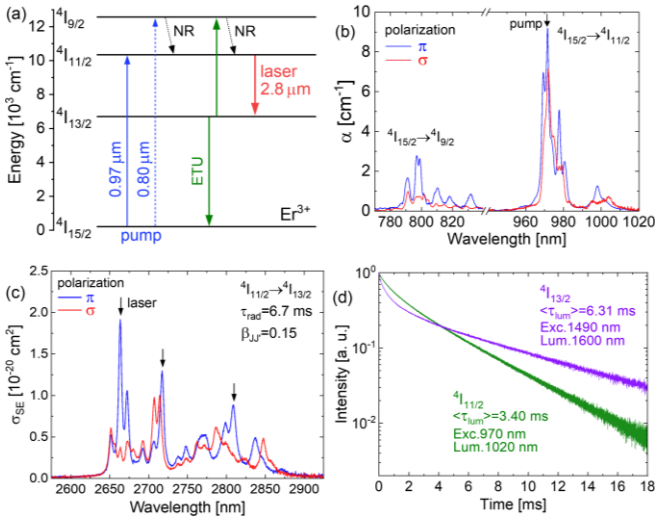

FIG. 2. Spectroscopy of Er:$LiYF_4$ epitaxial layers: (a) a simplified scheme of energy-levels of Er^{3+} ions, ETU – energy-transfer upconversion, NR – non-radiative decay; (b) polarized absorption spectra, the $^4I_{15/2} \rightarrow {}^4I_{11/2}$ and $^4I_{9/2}$ transitions; (c) SE cross-sections, σ_{SE}, the $^4I_{11/2} \rightarrow {}^4I_{13/2}$ transition. Light polarizations: π and σ. *Arrows* indicate the pump and laser wavelengths (for π polarized light); (d) luminescence decay curves from the $^4I_{11/2}$ and $^4I_{13/2}$ manifolds measured under resonant excitation.

The refractive index contrast $\Delta n = n_{layer} - n_{substrate}$ was estimated to be ~2×10^{-3} at ~2.8 μm owing to the effect of heavy Er^{3+} doping ($n_{substrate}$=1.458 for *e*-wave), based on the previous measurements for $LiYF_4$ layers with different rare-earth doping using a prism coupling technique. The planar WG supported two modes (TM_0 and TM_1) at the laser wavelength of 2.8 μm.

The layout of the WG laser set-up is depicted in Fig. 3(a). The laser WG, 10.6 at.% Er:$LiYF_4$, had a length of 2.8 mm, a width of 5 mm, and a layer thickness of 40 μm. It was mounted on a passively cooled Cu-holder using a silver paint. The linear cavity comprised a plane pump mirror (PM) coated for high transmission at the pump wavelength (T > 99% at 0.97 μm) and high reflectance (HR) at 2.6–3.0 μm, and two different plane output couplers (OCs) with a transmission T_{OC} of 1.7% or 4.0% at 2.65-2.95 μm. Both mirrors were slightly pressed towards the WG end facets resulting in a cavity length of a few millimeters. This helped to eliminate the intracavity losses due to the structured water vapor absorption in the air at the laser wavelength. The pump source was a Ti:Sapphire laser (model 3900S, Spectra Physics) delivering up to 2.7 W at 971 nm with a nearly diffraction limited beam quality ($M^2 \approx 1$). It addressed the $^4I_{15/2} \rightarrow {}^4I_{11/2}$ Er^{3+} absorption band. The pump radiation was focused on the input waveguide end-facet through the PM using an uncoated CaF_2 lens (focal length: f = 40 mm) resulting in a measured spot diameter of 28 μm. The pump polarization was adjusted by an antireflection coated half-wave plate, and it corresponded to π in the layer. The pump coupling efficiency was estimated from a transmission experiment at 875 nm (out of Er^{3+} absorption). It amounted to 94% (Fresnel losses from the WG end facet excluded). This value also accounts for the WG propagation loss. The pump absorption efficiency at 971 nm was measured by the end-fire method. It amounted to 67% at low pump powers (the small-signal value), and saturated at high pump levels due to the ground-state bleaching, Fig. 3(b). The residual pump after the OC was filtered out using a long-pass filter (LP2440, Spectrogon). The spectra of laser emission were measured using a ZrF_4 fiber and an OSA (AQ6376, Yokogawa). The near-field mode profile of the laser radiation was captured using a CaF_2 lens (f = 15 mm) and a pyroelectric camera (PY-III-HR-C-A, Ophir-Spiricon). The temporal dynamics of laser emission was monitored using a photodetector (UM-I-10.6, Vigo Photonics) and an 8-GHz digital oscilloscope.

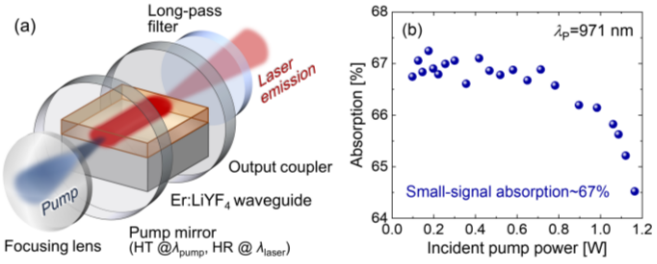

FIG. 3. (a) Layout of the Er:$LiYF_4$ planar waveguide laser; (b) measured pump absorption efficiency under non-lasing conditions, λ_P = 971 nm, π-polarization.

The continuous-wave (CW) Er:$LiYF_4$ planar WG laser generated a maximum output power of 191 mW at 2.81 μm with a slope efficiency η of 15% (versus the absorbed pump power) and a laser threshold of 134 mW when using 4.0% OC, Fig. 4(a). With lower output coupling of 1.7%, the WG laser exhibited a lower threshold of 79 mW whilst delivering 42 mW at 2.72 μm with a slope efficiency of 3.3%. The output dependencies were linear, and no signs of detrimental thermal effects nor damage were observed. Further power scaling was limited by the available pump.

The typical laser emission spectra are shown in Fig. 4(b,c). Near the threshold, the WG laser operated at 2663 nm for both OCs. By increasing the pump power, additional laser lines appeared at longer wavelengths of 2717 nm and 2809 nm, and well above the laser threshold, they dominated in the spectra. The observed laser lines correspond to local maxima in the SE cross-section spectra as shown by arrows in Fig. 2(c). The laser polarization was linear (π) being in line with the gain anisotropy. The observed red-shift of the laser wavelength with increasing the pump intensity is due to the stronger reabsorption from the terminal laser manifold caused by a resonant excited-state absorption (ESA), $^4I_{13/2} \rightarrow {}^4I_{11/2}$. The ESA from the $^4I_{13/2}$ manifold could be significant due to its relatively long luminescence lifetime.

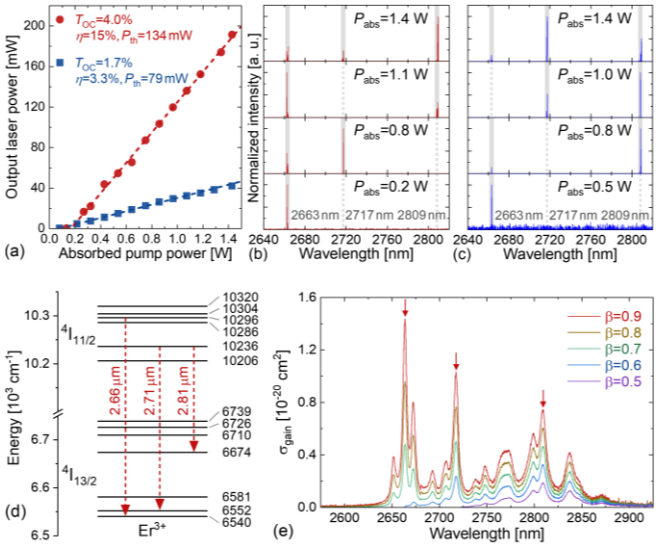

FIG. 4. Er:$LiYF_4$ planar waveguide laser: (a) input-output dependences, η – slope efficiency and P_{th} – laser threshold power; (b,c) typical spectra of laser emission taken at various absorbed pump powers P_{abs} for (b) T_{OC} = 4.0% and (c) T_{OC} = 1.7%, the laser polarization is π; (d) crystal-field splitting of the $^4I_{11/2}$ and $^4I_{13/2}$ multiplets, *arrows* – assignment of the observed laser lines; (e) gain cross-sections, σ_{gain}, around 2.8 μm, for various inversion ratios β, *arrows* - laser wavelengths.

To explain the observed spectral behavior, we calculated the ESA cross-sections, σ_{ESA}, of Er^{3+} ions using the reciprocity method[25] based on the σ_{SE} spectra, cf. Fig. 2(c), and experimental crystal-field splitting of the $^4I_{13/2}$ and $^4I_{11/2}$ manifolds depicted in Fig. 4(d), following the approach

presented in [26]. The maximum σ_{ESA} of 2.86×10^{-20} cm^2 is found at 2663 nm for π-polarized light. The gain cross-sections, $\sigma_{gain} = \beta\sigma_{SE} - (1-\beta)\sigma_{ESA}$, were further determined in analogy to quasi-three-level gain media with reabsorption from the terminal laser level, where $\beta = N_3 / (N_2 + N_3)$ stands for the population inversion ratio, and N_1, N_2 and N_3 are the populations of the $^4I_{15/2}$, $^4I_{13/2}$ and $^4I_{11/2}$ manifolds, respectively ($N_1 + N_2 + N_3 \approx N_{Er}$), see Fig. 4(e). The actual β value for the developed Er waveguide laser was estimated to be about 0.85 by solving the rate equations accounting for the pump rate, spontaneous decay, and ETU. For such high inversion ratios, one can see three dominant peaks in the gain spectra well matching the observed laser lines. They were further assigned to electronic transitions based on the Stark energy-level structure of Er^{3+} ions, see Fig. 4(d).

The observed near-field profiles of the guided pump and laser modes are shown in Fig. 5(a). The pump mode at the output facet of the waveguide is strongly elliptical due to the free propagation in the horizontal direction and a strong light confinement along the vertical axis. The laser mode also has a clear fingerprint of the planar WG geometry. The laser mode was nearly diffraction limited in the vertical direction.

A typical oscilloscope trace of laser emission at 2.8 μm is shown in Fig. 5(b). After switching on the pump, it clearly represents the spiking, damping and relaxation oscillation behaviors followed by a stable CW operation regime. From the measured frequency of relaxation oscillations (f ~240 kHz at P_{abs} = 1.43 W), the passive intracavity losses including the WG propagation loss could be estimated by a rate-equation modeling of the laser[27] yielding a round-trip loss of about 5%.

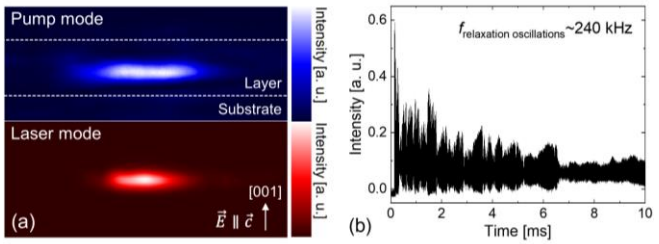

FIG. 5. Er:$LiYF_4$ planar waveguide laser: (a) the near-field guided pump and laser modes (not in scale), the laser polarization (π) is vertical; (b) an oscilloscope trace of laser emission showing spiking and relaxation oscillations, T_{OC}=1.7%, P_{abs}=1.43 W.

The output of the Er:$LiYF_4$ WG laser was simulated using a model of a quasi-three-level laser (with reabsorption) accounting for the ESA from terminal laser level. The determined spectroscopic parameters were used. This provided an estimate of the round-trip passive loss of 5±1% (the WG propagation loss: 0.4±0.2 dB/cm).

Recently, channel laser WGs were produced in 11-mm-long bulk Er:$LiYF_4$ crystals by ULI.[15] The fs-laser written microstructure consisted of 56 tracks exhibiting a refractive index contrast of 0.7×10^{-3}. The WG laser generated 66 mW at 2.81 μm with a laser threshold of 120 mW. The advantages of LPE based WGs include (i) easier control of the refractive index contrast for efficient waveguiding towards single transverse mode behavior as well as (ii) better thermal management leading to better power scaling capabilities.

To conclude, we report on the first mid-infrared laser operation of heavily Er^{3+}-doped $LiYF_4$ single-crystalline layers elaborated by LPE in the planar WG geometry. The grown Er^{3+}-doped layers present high quality (WG propagation loss: 0.4±0.2 dB/cm) and a uniform dopant distribution, as well as a refractive index contrast of Δn ~2×10^{-3} leading to a strong confinement of both the pump and laser modes. The output power is scaled up to 191 mW with a slope efficiency of 15% when using 4.0% OC transmission and a laser threshold down to 79 mW is observed for smaller output coupling of 1.7%. The laser spectra exhibit several emission lines around 2.8 μm in agreement with polarized stimulated-emission properties of Er^{3+} ions.

Further improvement of the laser performance is expected by optimizing the Er^{3+} doping level to boost the ETU efficiency (growth of layers doped with tens of at.% Er^{3+} is feasible), as well as the layer quality with the goal of further reducing the propagation losses. Micro-structuring of such layers by precision diamond saw dicing[19] is expected to lead to channel (ridge) WGs featuring a single-transverse-mode behavior and higher laser efficiencies and lower laser thresholds due to the stronger light confinement and better overlap of the pump and laser modes. The demonstrated Er:$LiYF_4$ WG laser platform is also anticipated to be monolithically combined with saturable absorbers for pulsed operation such as passive Q-switching and mode-locking. Surface WGs can be functionalized via deposition of a nonlinear material for evanescent-field interaction. The monolithic WG laser design helps to ultimately reduce the intracavity water vapor absorption (as compared to standard solid-state laser cavities with free-space propagation) which is of primary importance for ultrashort pulse generation at 2.8 μm.

ACKNOWLEDGMENTS

The work was supported by the Agence Nationale de la Recherche (SPLENDID2, ANR-19-CE08-0028), Région Normandie (Chaire d'excellence "RELANCE"), and Horizon 2020 Marie Skłodowska-Curie Actions (101034329).

DATA AVAILABILITY

The data that support the findings of this study are available from the corresponding author upon reasonable request.

REFERENCES

[1]C. Grivas, R. Ismaeel, C. Corbari, C.-C. Huang, D. W. Hewak, P. Lagoudakis, and G. Brambilla, "Generation of multi-gigahertz trains of phase-coherent femtosecond laser pulses in Ti:sapphire waveguides," Laser Photonics Rev. **12**(11), 1800167 (2018).

[2]X. Jiang, H. Lu, Q. Li, H. Zhou, S. Zhang, and H. Zhang, "Epsilon-near-zero medium for optical switches in a monolithic waveguide chip at 1.9 μm," Nanophoton. **7**(11), 1835–1843 (2018).
[3]J. E. Bae, X. Mateos, M. Aguiló, F. Díaz, J. G. Ajates, C. Romero, J. R. V. de Aldana, and F. Rotermund, "Multi-gigahertz mode-locked femtosecond Yb:KLuW waveguide lasers," Photonics Res. **10**(11), 2584–2589 (2022).
[4]A. Schliesser, N. Picqué, and T. W. Hänsch, "Mid-infrared frequency combs," Nat. Photon. **6**(7), 440–449 (2012).
[5]J. Ma, Z. Qin, G. Xie, L. Qian, and D. Tang, "Review of mid-infrared mode-locked laser sources in the 2.0 μm–3.5 μm spectral region," Appl. Phys. Rev. **6**(2), 021317 (2019).
[6]F. Chen and J. R. V. de Aldana, "Optical waveguides in crystalline dielectric materials produced by femtosecond-laser micromachining," Laser Photonics Rev. **8**(2), 251-275 (2014).
[7]P. A. Berry, J. R. Macdonald, S. J. Beecher, S. A. McDaniel, K. L. Schepler, and A. K. Kar, "Fabrication and power scaling of a 1.7 W Cr:ZnSe waveguide laser," Opt. Mater. Express. **3**(9), 1250–1258 (2013).
[8]J. R. Macdonald, S. J. Beecher, A. Lancaster, P. A. Berry, K. L. Schepler, A. K. Kar, "Ultrabroad mid-infrared tunable Cr:ZnSe channel waveguide laser," IEEE J. Sel. Top. Quantum Electron. **21**(1), 1601405 (2015).
[9]A. Lancaster, G. Cook, S. A. McDaniel, J. Evans, P. A. Berry, J. D. Shephard, and A. K. Kar, "Mid-infrared laser emission from Fe:ZnSe cladding waveguides," Appl. Phys. Lett. **107**(3), 031108 (2015).
[10]D. G. Lancaster, D. E. Otten, A. Cernescu, N. Bourbeau Hébert, G. Y. Chen, C. M. Johnson, T. M. Monro, and J. Genest, "An ultra-stable 2.9 μm guided-wave chip laser and application to nano-spectroscopy," APL Photon. **4**(11), 110802 (2019).
[11]Y.-P. Peng, X. Zou, Z. Bai, Y. Leng, B. Jiang, X. Jiang, and L. Zhang, "Mid-infrared laser emission from Cr:ZnS channel waveguide fabricated by femtosecond laser helical writing," Sci. Rep. **5**, 18365 (2015).
[12]J. R. Macdonald, S. J. Beecher, P. A. Berry, G. Brown, K. L. Schepler, and A. K. Kar, "Efficient mid-infrared Cr:ZnSe channel waveguide laser operating at 2486 nm," Opt. Lett. **38**(13), 2194–2196 (2013).
[13]D. G. Lancaster, S. Gross, H. Ebendorff-Heidepriem, M. J. Withford, T. M. Monro, and S. D. Jackson, "Efficient 2.9 μm fluorozirconate glass waveguide chip laser," Opt. Lett. **38**(14), 2588–2591 (2013).
[14]Q. Tian, P. Yin, T. Zhang, L. Zhou, B. Xu, Z. Luo, H. Liu, Y. Ge, J. Zhang, P. Liu, and X. Xu, "MXene $Ti_3C_2T_x$ saturable absorber for passively Q-switched mid-infrared laser operation of femtosecond-laser–inscribed Er:Y_2O_3 ceramic channel waveguide," Nanophoton. **9**(8), 2495–2503 (2020).
[15]B. Ayevi, Y. Morova, M. Tonelli, and A. Sennaroglu, "Er^{3+}:$YLiF_4$ channeled waveguide laser near 2.7–2.8 μm fabricated by femtosecond laser inscription." Opt. Lett. **49**(4), 1017–1020 (2024).
[16]M. R. Majewski, M. Pawliszewska, and S. D. Jackson, "Picosecond pulse formation in the presence of atmospheric absorption," Opt. Express **29**(12), 19159–19169 (2021).
[17]R. Švejkar, J. Šulc, M. Němec, and H. Jelínková, "Compact diode-pumped CW and Q-switched 2.8 μm Er:YLF laser," J. Opt. Soc. Am. B **38**(8), B26–B29 (2021).
[18]W. Bolaños, J. J. Carvajal, X. Mateos, G. S. Murugan, A. Z. Subramanian, J. S. Wilkinson, E. Cantelar, D. Jaque, G. Lifante, M. Aguiló, and F. Díaz, "Mirrorless buried waveguide laser in monoclinic double tungstates fabricated by a novel combination of ion milling and liquid phase epitaxy," Opt. Express **18**(26), 26937–26945 (2010).
[19]K. van Dalfsen, S. Aravazhi, D. Geskus, K. Wörhoff, and M. Pollnau, "Efficient $KY_{1-x-y}Gd_xLu_y(WO_4)_2$:$Tm^{3+}$ channel waveguide lasers," Opt. Express **19**(6), 5277–5282 (2011).
[20]P. Loiko, R. Soulard, G. Brasse, J.-L. Doualan, B. Guichardaz, A. Braud, A. Tyazhev, A. Hideur, and P. Camy, "Watt-level Tm:$LiYF_4$ channel waveguide laser produced by diamond saw dicing," Opt. Express **26**(19), 24653–24662 (2018).
[21]J. E. Williams, V. V. Fedorov, D. V. Martyshkin, I. S. Moskalev, R. P. Camata, and S. B. Mirov, "Mid-IR laser oscillation in Cr^{2+}:ZnSe planar waveguide," Opt. Express **18**(25), 25999–26006 (2010).
[22]W. Bolanos, F. Starecki, A. Benayad, G. Brasse, V. Ménard, J.-L. Doualan, A. Braud, R. Moncorgé, and P. Camy, "TmLiYF_4 planar waveguide laser at 1.9 μm," Opt. Lett. **37**(19), 4032–4034 (2012).
[23]L. Basyrova, G. Brasse, P. Loiko, C. Grygiel, R. M. Solé, M. Aguiló, F. Díaz, X. Mateos, A. Benayad, J.-L. Doualan, and P. Camy, "Liquid phase epitaxy growth and structural characterization of highly-doped Er^{3+}:$LiYF_4$ thin films," Opt. Mater. **132**, 112574 (2022).
[24]C. Li, Y. Guyot, C. Linatès, R. Moncorgé, and M. F. Joubert, "Radiative Transition Probabilities of Trivalent Rare-Earth Ions in LiYF4," Paper NL7, OSA Proceedings series on Advanced Solid State Lasers 15, 91–95 (1993).
[25]S. A. Payne, L. L. Chase, L. K. Smith, W. L. Kway, and W. F. Krupke, "Infrared cross-section measurements for crystals doped with Er^{3+}, Tm^{3+} and Ho^{3+}," IEEE J. Quantum Electron. **28**(11), 2619–2630 (1992).
[26]F. Cassouret, A. Nady, P. Loiko, S. Normani, A. Braud, W. Chen, V. Petrov, D. Sun, P. Zhang, B. Viana, A. Hideur, and P. Camy, "Polarization switching in a mid-infrared Er:$YAlO_3$ laser," Opt. Lett. **49**(11), 2970–2973 (2024).
[27]J. E. Bae, M. Hyun, D. W. Kim, X. Mateos, J. G. Ajates, C. Romero, J. R. V. de Aldana, J. Kim, and F. Rotermund, "Characterization of noise spectra in low-jitter GHz mode-locked fs-laser-inscribed waveguide lasers," Opt. Laser Technol. **179**, 111412 (2024).